

W51 IRS 2: A MASSIVE JET EMERGING FROM A MOLECULAR CLOUD INTO AN H II REGION

JOHN H. LACY¹, DANIEL T. JAFFE¹, QINGFENG ZHU², MATTHEW J. RICHTER³, MARTIN A. BITNER¹, THOMAS K. GREATHOUSE⁴, KEVIN VOLK⁵, T. R. GEBALLE⁵, AND DAVID M. MEHRINGER⁶

Draft version July 4, 2018

ABSTRACT

We have mapped [Ne II] (12.8 μm) and [S IV] (10.5 μm) emission from W51 IRS 2 with TEXES on Gemini North, and we compare these data to VLA free-free observations and VLT near-infrared images. With 0.5'' spatial and 4 km s⁻¹ spectral resolution we are able to separate the ionized gas into several components: an extended H II region on the front surface of the molecular cloud, several embedded compact H II regions, and a streamer of high velocity gas. We interpret the high velocity streamer as a precessing or fan-like jet, which has emerged from the molecular cloud into an OB star cluster where it is being ionized.

Subject headings: H II regions—ISM: jets and outflows—ISM: infrared

1. INTRODUCTION

Most star formation, across the IMF, takes place in massive star-forming cores (Lada & Lada 2003). The disruption of these cores as high mass stars form terminates the formation of low and intermediate mass stars and is a major contributor to the dynamical energy in the dense ISM. While much of this disruption results from the ionization of H II regions and their subsequent expansion, it is becoming increasingly evident that dynamically significant amounts of supersonic gas are present during the very early phases of core dissipation (De Pree et al. 2004). In this paper we present observations of a jet containing a significant fraction of the kinetic energy of an expanding H II region.

W51 IRS 2, which includes the compact H II region W51d and the maser complex W51 NORTH, lies within the H II region complex G49.5-0.4 in W51A, a very luminous region of massive young stars and molecular and ionized gas (Bieging 1975; Genzel et al. 1982; Carpenter & Sanders 1998). The distance to W51 NORTH has been determined from H₂O maser proper motion studies to be 6-8 kpc (Genzel et al. 1981; Schneps et al. 1981; Imai et al. 2002), which is consistent with the far kinematic distance for the molecular cloud velocity of 57 km s⁻¹. We will use a distance of 7 kpc, at which 1 pc subtends 30''.

Radio free-free and recombination line observations of W51 have been made by Martin (1972), Gaume et al. (1993), and Mehringer (1994). The 3.6 cm free-free image of IRS 2 shown in Mehringer (1994, Figure 19) is from observations using all four VLA configurations, which preserves both large and small scale structure. We show a larger portion of that image in Figure 1 (Plate x) and

the IRS 2 region in Figure 2a. Various names have been given to the emission peaks in IRS 2. We will refer to the free-free peaks labeled a-f in Figure 2a as IRS 2a-2f, and the compact infrared continuum source as 2i. Our IRS 2a and 2b have been called W51d₁, our 2d is W51d, and our 2e is W51d₂.

Okamoto et al. (2001) observed infrared fine-structure line emission of [Ne II] (12.8 μm), [Ar III] (9.0 μm), and [S IV] (10.5 μm) from the ionized gas, and concluded that the gas is ionized by radiation from stars of spectral type O8-O9. At 7 kpc, the ionized gas in IRS 2 requires a Lyman continuum luminosity of 6.5×10^{49} sec⁻¹ (Martin 1972), and the luminosity of IRS 2 is $2 - 4 \times 10^6$ L_⊙ (Erickson & Tokunaga 1980; Jaffe et al. 1985).

Near-infrared observations show a cluster of young stars coincident with IRS 2 containing 2-8 times as many ionizing stars as the trapezium cluster (Goldader & Wynn-Williams 1994; Hodapp & Davis 2002). Stellar colors indicate an extinction of A_V ~ 25 mag. An H-band adaptive optics image with 0.05'' resolution, with the 3.6 cm contours overlaid, is shown in Figure 1b. This image was taken with NAOS-Conica on the VLT Yepun as part of program 71.C-0344(A), and was obtained from the VLT archive. Most of the point sources are stars in the IRS 2 cluster. The diffuse emission correlates rather well with the 3.6 cm emission, although it appears to be cut off on the northern side, with the northeastern half of the IRS 2d missing, probably because of extinction. The diffuse H-band emission probably is dominated by H I Brackett series lines.

The W51 NORTH maser group includes H₂O, OH, SiO, and NH₃ masers. The majority of the H₂O maser peaks are in the ‘dominant center’ group (Schneps et al. 1981; Imai et al. 2002, ‘m’ in Fig. 2a), which is centered on a more compact cluster of SiO masers (Eisner et al. 2002) and on the peak of the thermal NH₃ emission (Ho et al. 1983).

2. OBSERVATIONS

We observed W51 IRS 2 during the Texas Echelon Cross Echelle Spectrograph (TEXES) Demonstration Science run on the 8-m Gemini North telescope in July 2006. TEXES is a high resolution cross-dispersed mid-infrared (5-25 μm) spectrograph capable of 0.4'' and

¹ Department of Astronomy, The University of Texas at Austin, Austin, TX 78712; lacy, dtj, mbitner@astro.as.utexas.edu

² Center for Imaging Science, Rochester Institute of Technology, Rochester, NY 14623; qxzpci@cis.rit.edu

³ Department of Physics, University of California, Davis, CA 95616; richter@physics.ucdavis.edu

⁴ Lunar and Planetary Institute, Houston, TX 77058, greathouse@lpi.usra.edu

⁵ Gemini Observatory, Hilo, HI 96720; kvolk, tgeballe@gemini.edu

⁶ davemehring@yaho.com

3 km s⁻¹ resolution on Gemini (Lacy et al. 2002). All data from the Science Demonstration run are available from the Gemini archive at <http://archive.gemini.edu>. Members of the astronomical community are welcome to propose to use TEXES. We expect it to be available in alternating semesters on Gemini and the IRTF.

The observations presented here were made with a 0.6'' slit width and 0.15'' sampling along the slit. W51 IRS 2 was mapped at three spectral settings: 10.5 μm, including the 951.43 cm⁻¹ [SIV] line; 12.8 μm, including the 780.42 cm⁻¹ [Ne II] line; and 13.1 μm, including the 763.23 cm⁻¹ [Ar V] line. The maps were made by stepping the 4''-long N-S slit in 0.15'' steps across 12'' in R.A. Overlapping scans were made to cover 9'' in DEC at 10.5 μm and 7'' at 12.8 μm. An additional ten points were observed at the beginning of each scan to measure the sky background.

A map of the 12.8 μm continuum, from an 0.6 cm⁻¹ interval next to the [Ne II] line, is shown in Figure 2b. The [SIV] and [Ne II] line intensities, integrated over Doppler ranges of $v_{\text{LSR}} = -80$ to $+80$ km s⁻¹, with continuum subtracted, are shown in Figures 2c and 2d. The [Ne II] image is similar to the radio free-free image (Fig. 2a), with peaks seen at the positions of IRS 2a-c and possibly 2e-f. A bright peak is seen on the south edge of IRS 2d, but the northeast side of 2d is weak or absent in all of our maps. The [SIV] map is somewhat different, with IRS 2a and 2b absent and 2d even more cut off. With these bright sources suppressed, 2c and the extended emission covering most of the region mapped are more prominent in [SIV]. The [Ar V] line was undetected, and must be fainter than [Ne II] by a factor of at least 30.

Our continuum maps are consistent with those of Okamoto et al. (2001), who derive a silicate feature optical depth of $\tau_{9.7} \approx 2$ toward most of the ionized gas, implying a reddening between our lines of $E_{10.5-12.8} \approx 1$. Given the rather uniform reddening, except toward IRS 2i, where it is much larger, the differences between the [Ne II] and [SIV] maps must be due primarily to excitation or density differences. Of these two lines, [Ne II] normally dominates in gas excited by stars of spectral type O8 and later, and [SIV] dominates in gas excited by earlier type stars. However, [SIV] has a critical density for thermalization more than an order of magnitude less than [Ne II], decreasing the [SIV]/[Ne II] ratio in gas with $n_e > 10^4$ cm⁻³. IRS 2a and 2b, and the south edge of 2d, with [SIV]/[Ne II] < 1/3, are of relatively low excitation (or high density), whereas 2c and the extended emission have [SIV]/[Ne II] ≈ 3 .

The fits format data cubes are available from the Gemini archive. We show several position-velocity diagrams from the [SIV] cube in Figure 3 and broad channel maps in Figure 4. Movies of the P-V diagrams and maps are available on-line. The locations of the P-V cut lines are shown in Figure 2c. The Doppler shift of the positive velocity emission is close to that of the IRS 2 molecular cloud. There is a trend that the positive velocity emission toward center of the map is more redshifted than that near the edges. The emission near the center is redshifted from the ambient molecular gas by a few km s⁻¹. That near the edges is blueshifted by ~ 20 km s⁻¹. The most striking aspect of the P-V diagrams is the wide range in Doppler shift seen near and south of IRS 2c.

The 2c emission ridge is blueshifted from the ambient gas by ~ 110 km s⁻¹. This emission was seen by Mehringer (1994) in the H92α line, but was not resolved spatially, and the bridge between the blueshifted and ambient emission was not apparent. This 'bridge' emission makes it clear that the blueshifted gas is not just superimposed along the line of sight, but is interacting with the ambient gas. This is especially clear in P-V cut c, in which the Doppler shift of the ambient gas shifts to the blue where it connects into the bridge gas, and there is a gap in the ambient gas in the region where the bridge is strongest.

3. INTERPRETATION

Gas at Doppler shifts near that of the molecular cloud is seen throughout the region observed. Given the presence of a cluster of massive young stars centered on this region, we identify the extended gas as the surface of the cloud which is ionized by stellar UV. The moderate extinction to the gas and stars indicates that they lie near the front side of the cloud. The pattern of Doppler shifts ranging from just redward of the ambient cloud velocity near the center of the region and blueward toward the edges is consistent with a flow along a bowl-shaped front surface of the cloud. Zhu et al. (2005) show that the motion of the ionized gas in several compact H II regions can be explained in this way, and they suggest that such a flow can result, at least in part, from the pressure gradient in ionized gas compressed by the ram pressure of stellar winds. The [SIV]/[Ne II] ratio indicates that the gas is ionized by stars of spectral type O8 or earlier.

The large reddening of IRS 2i suggests that it lies within the molecular cloud behind the ionized gas. In addition, 2a and 2b must be separate from the rest of the ionized gas, given their relatively low excitation, indicating ionization by \sim O9 stars. However, this gas must not be very deeply embedded and could even be in a foreground cloud. Several of the brightest stars in Figure 1b lie near ionized gas peaks, suggesting that the star cluster is still partially embedded.

The explanation for the highly blueshifted gas in IRS 2c is not so clear, but the presence of 'bridge' gas at intermediate velocities connecting the ambient velocity and blueshifted emission in Figure 3 suggests that the blueshifted gas is in some sort of a jet that passed through the ionized surface of the molecular cloud. The jet must be neutral (to be unseen in the ionic lines) while inside of the cloud and probably is ionized by stellar UV when it emerges from the cloud. The presence of high velocity H₂O and SiO maser peaks 1'' south of 2c (near the Figure 3b cut line) suggests that the jet is a part of the same outflow as that in which the masers form. If this is the case, the jet must have precessed by $\sim 90^\circ$ since the gas we see was emitted, since the masers are moving near the plane of the sky in an approximately E-W bipolar pattern, whereas the ionized jet is to the north of the maser center and has a substantial velocity component toward us. However, the ionized jet may not be the same as the one responsible for the 'dominant center' maser peaks. There are several other groups of masers in IRS 2, which suggests that there are several outflow centers. We may be able to localize better the origin of the outflow we see from the information in the [SIV] data cube. Just south of 2c there is a gap in the cloud surface gas shown in Figure 4a, which could be caused by the passage of the

jet through the surface H II region. If it is, the source of the jet must lie farther to the south, and so to the south of the maser center. Observations of a neutral jet tracer, such as shocked H₂, could localize the source and test this interpretation.

The E-W elongation of the blueshifted emission could be a result of the precession of a narrowly collimated jet, or the gas could have been emitted in a fan. In either case, the relatively small variation in the Doppler shift at the peak of the emission along the blueshifted jet suggests that the angle of the jet to our line of sight does not vary by a large amount along its length. This indicates that the distance along our line of sight to the source of the jet is at least several times greater than the 0.13 pc length of the blueshifted emission. We can estimate the time since the jet was emitted from the ratio of the distance to the ionized jet from its source to the observed velocity. This gives a time of >1200 yr.

The extent of the intermediate velocity ‘bridge’ gas in Figures 3 and 4 is something of a puzzle. The narrowness of the blueshifted ridge indicates that the jet responsible for it is well collimated, at least in declination. But the extent of the bridge emission is almost as great in declination as it is in right ascension. Two explanations seem plausible. As the surface of the jet is photoionized, it would be expected to expand, and it might slow down by interaction with the surrounding medium. Alternatively, the jet might carry along with it material from the H II layer on the surface of the molecular cloud. Williams (2004) has suggested that a turbulent magnetized medium should act as a visco-elastic fluid. It would be interesting to ask whether this effect could be strong enough to account for the acceleration of the bridge gas.

We can estimate the mass of the ionized gas in the blueshifted emission from the ionic line fluxes. Okumura et al. (2001) derived an electron density in the ionized gas in IRS 2 of $10^5 - 10^6 \text{ cm}^{-3}$ from the ratio of near-infrared [Fe III] lines. At that density, the [S IV] line should be thermalized, making its flux proportional to mass. We then calculate the mass of ionized gas in the jet to be $3 \times 10^{-3} M_{\odot}$ assuming all of the S is S⁺³, and S/H is solar. Since some of the gas may be in other ionization states (in fact the core of the jet most likely is neutral, at least when it emerges from the molecular

cloud), this mass estimate is a lower limit. Assuming the ionized part of the jet includes gas emitted over 500 yr, we obtain a bipolar mass flow of $> 1.2 \times 10^{-5} M_{\odot} \text{ yr}^{-1}$ and an energy flow of $> 10 L_{\odot}$. For comparison, molecular outflows from massive young stars range upward from $3 \times 10^{-5} M_{\odot} \text{ yr}^{-1}$ (Garay & Lizano 1999).

The high velocity streamer in W51 is similar to the irradiated Herbig-Haro jets seen by Reipurth et al. (1998) and Cernicharo et al. (1998), but has an emission measure a factor of 10^5 greater than those of the irradiated jets in the Orion nebula (Bally & Reipurth 2001) and a mass flow rate a factor of at least 10^4 greater than those jets. It more closely resembles the HH 80-81 bipolar jet (Marti, Rodriguez & Reipurth 1993), which comes from a massive star. The HH 80-81 jet has much greater extent than that in W51, but is not as luminous in ionic emission, likely due to the lack of as strong of a source of ionizing radiation. It is highly collimated and shows some evidence of precession, although not as much as we suggest for the W51 jet.

We thank the Gemini staff, especially John White, for their outstanding help in making TEXES work on Gemini North. We also thank Jim Umbarger for assistance with the figures. The development of TEXES was supported by grants from the NSF and the NASA/USRA SOFIA project. The modification of TEXES for use on Gemini was supported by Gemini Observatory. Observations with TEXES were supported by NSF grant AST-0607312. This work is based on observations obtained at the Gemini Observatory, which is operated by the Association of Universities for Research in Astronomy, Inc., under a cooperative agreement with the NSF on behalf of the Gemini partnership: the National Science Foundation (United States), the Particle Physics and Astronomy Research Council (United Kingdom), the National Research Council (Canada), CONICYT (Chile), the Australian Research Council (Australia), CNPq (Brazil), and CONICET (Argentina). The near-infrared image in Figure 2b is based on observations with the European Southern Observatory telescopes obtained from the ESO/ST-ECF Science Archive Facility.

REFERENCES

- Bally, J. and Reipurth, B. 2001, *ApJ*, 546, 299
 Bieging, J. 1975, in *H II Regions and Related Topics*, ed. T.L. Wilson and D. Downes (Berlin: Springer), 443
 Carpenter, J.M. and Sanders, D.B. 1998, *AJ*, 116, 1856
 Cernicharo, J. et al. 1998, *Science*, 282, 462
 De Pree, C.G., Wilner, D.J., Mercer, A.J., Davis, L.E., Goss, W.M., and Kurtz, S. 2004, *ApJ*, 600, 286
 Eisner, J.A., Greenhill, L.J., Herrnstein, J.R., Moran, J.M., and Menten, K.M. 2002, *ApJ*, 569, 334
 Erickson, E.F. and Tokunaga, A.T. 1980, *ApJ*, 238, 596
 Garay, G., and Lizano, S. 1999, *PASP*, 111, 1049
 Gaume, R.A., Johnston, K.J., and Wilson, T.L. 1993, *ApJ*, 417, 645
 Genzel, R. et al. 1981, *ApJ*, 247, 1039
 Genzel, R., Becklin, E.E., Wynn-Williams, C.G., Moran, J.M., Reid, M.J., Jaffe, D.T., and Downes, D. 1982, *ApJ*, 255, 527
 Goldader, J.D. and Wynn-Williams, C.G. 1994, *ApJ*, 433, 164
 Ho, P.T.P., Genzel, R. and Das, A. 1983, *ApJ*, 266, 596
 Hodapp, K. and Davis, C. 2002, *ApJ*, 575, 291
 Imai, H., Watanabe, T., Omodaka, T., Nishio, M., Kameya, O., Miyaji, T., and Nakajima, J. 2002, *PASJ*, 54, 741
 Jaffe, D.T., Genzel, R., Harper, D.A., Harris, A.I., and Ho P.T.P. 1985, in *IAU Symp 115: Star Forming Regions*, ed. M. Peimbert & J. Jugaku (D. Reidel: Dordrecht), 143
 Lacy, J.H., Richter, M.J., Greathouse, T.K., Jaffe, D.T., and Zhu, Q-F. 2002, *PASP*, 114, 153
 Lada, C.J., and Lada, E.A. 2003, *ARA&A*, 41, 57
 Marti, J., Rodriguez, L.F., and Reipurth, B. 1993, *ApJ*, 416, 208
 Martin, A. 1972, *MNRAS*, 157, 31
 Mehringer, D.M. 1994, *ApJS*, 91, 713
 Okumura, S., Mori, A., Watanabe, E., Nishihara, E., and Yamashita, T. 2001, *AJ*, 121, 2089
 Okamoto, Y.K., Kataza, H., Yamashita, T., Miyata, T., and Onaka, T. 2001, *ApJ*, 553, 245
 Reipurth, B., Bally, J., Fesen, R.A., and Devine, D. 1998, *Nature*, 396, 343
 Schneps, M.H., Lane, A.P., Downes, D., Moran, J.M., Genzel, R., and Reid, M.J. 1981, *ApJ*, 249, 124
 Williams, P.T. 2004, *NewA*, 10, 133
 Zhu, Q-F., Lacy, J.H., Jaffe, D.T., Richter, M.J., and Greathouse, T.K. 2005, *ApJ*, 631, 381

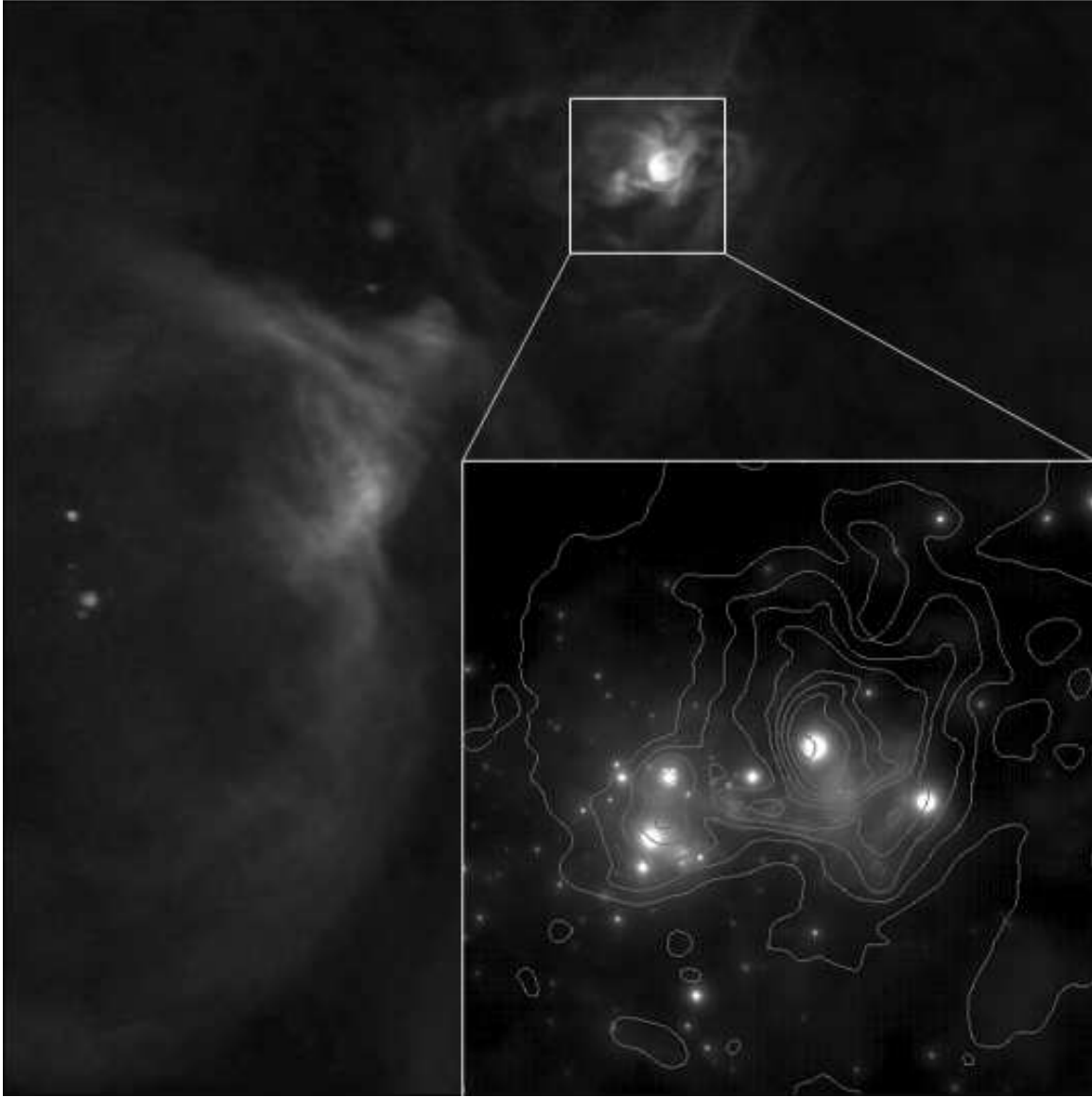


FIG. 1.— a) (background image) 3.6 cm free-free continuum emission from W51A (IRS 1 and IRS 2). IRS 2 is near the top of the image. The image was made from the VLA ABCD configuration data set described in Mehringer (1994). The grayscale uses a square-root stretch. The image extent is $112'' \times 112''$. b) (inset) H-band continuum emission from stars and ionized gas in IRS 2, with 3.6 cm contours superimposed. The H-band data were obtained from the ESO VLT archive. The grayscale and contours use a square-root stretch. The image extent is $15'' \times 15''$.

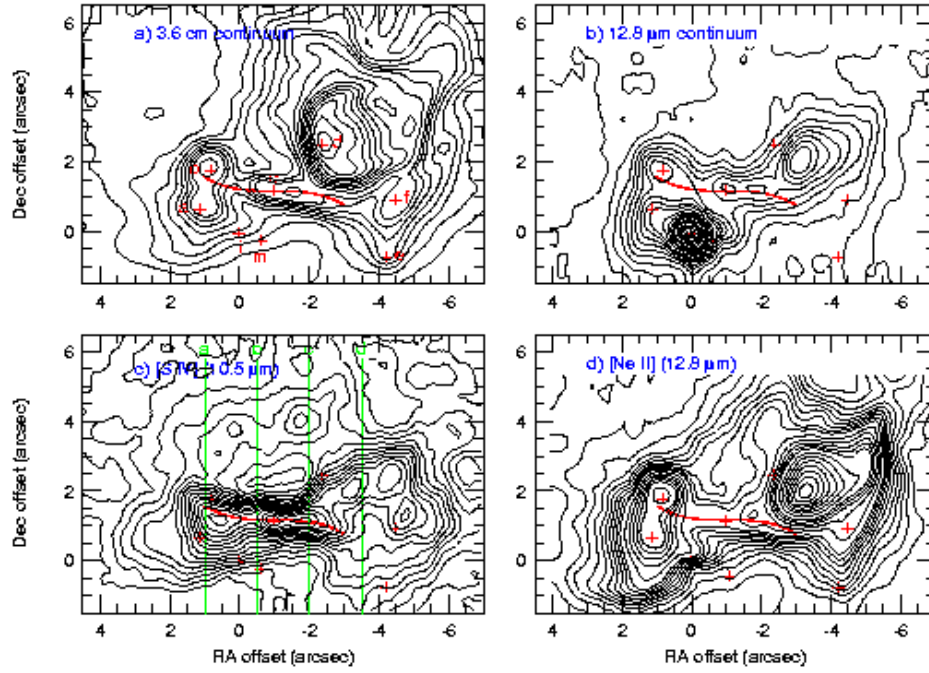


FIG. 2.— Radio free-free, infrared continuum, and infrared line maps of W51 IRS 2. Axes are labeled in arcseconds from the infrared continuum source IRS 2i at $19^{\text{h}}23^{\text{m}}40.10^{\text{s}} 14^{\circ}31'06.0''$ (J2000). a) 3.6 cm emission from Mehringer (1994), with various H II and maser peaks marked. Contours are at $1, 2, \dots, 8, 10, \dots, 26 \times 0.0025 \text{ Jy beam}^{-1}$ or $7.5 \times 10^9 \text{ Jy sr}^{-1}$. H II peaks marked a-f are referred to in the text as IRS 2a-f. The curve through c shows the region of blue-shifted emission. IRS 2i is the infrared continuum source, and m is the maser center. b) $12.8 \mu\text{m}$ continuum emission. Contours are at $1, 2, \dots, 10, 12, \dots, 20, 24, \dots, 44 \times 0.014 \text{ erg/s cm}^2 \text{ sr cm}^{-1}$. c) [S IV] ($10.5 \mu\text{m}$) line emission. Contours are at $1, 2, \dots, 15 \times 0.009 \text{ erg/s cm}^2 \text{ sr}$. Lines show locations of P-V cuts in Figure 3. d) [Ne II] ($12.8 \mu\text{m}$) line emission. Contours are at $1, 2, \dots, 10, 12, \dots, 20, 24, \dots, 48 \times 0.023 \text{ erg/s cm}^2 \text{ sr}$.

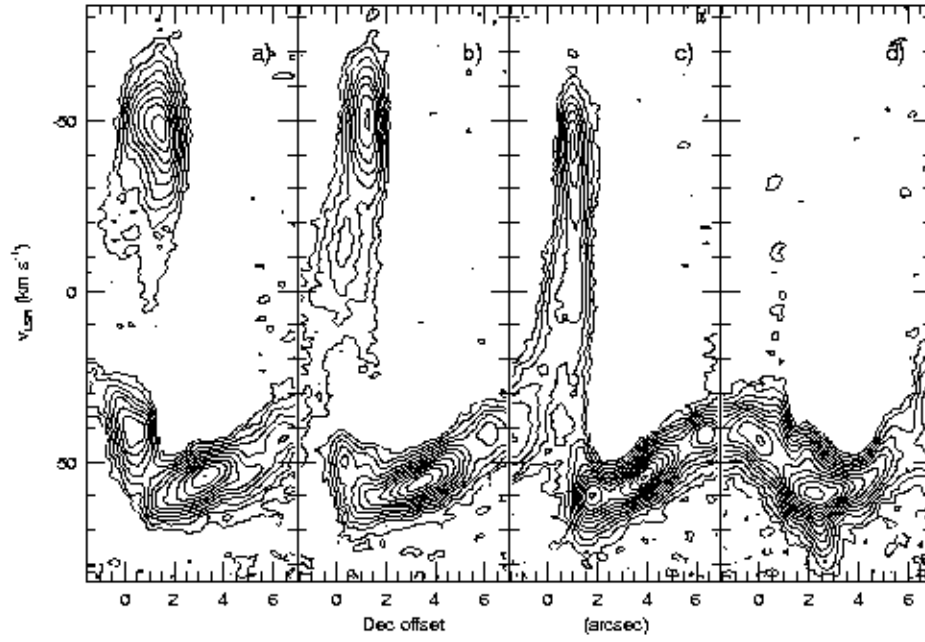


FIG. 3.— Position-velocity cuts through the [SIV] data cube. Horizontal axes are labeled in arcseconds north from IRS 2i. The contours are spaced quadratically. The ambient molecular cloud is near $v_{\text{LSR}} = 57 \text{ km s}^{-1}$. Locations of cut lines are shown in Figure 2c. The online movie shows the data cube as a sequence of P-V diagrams. The movie frames are labeled by the R.A. offset from IRS 2i.

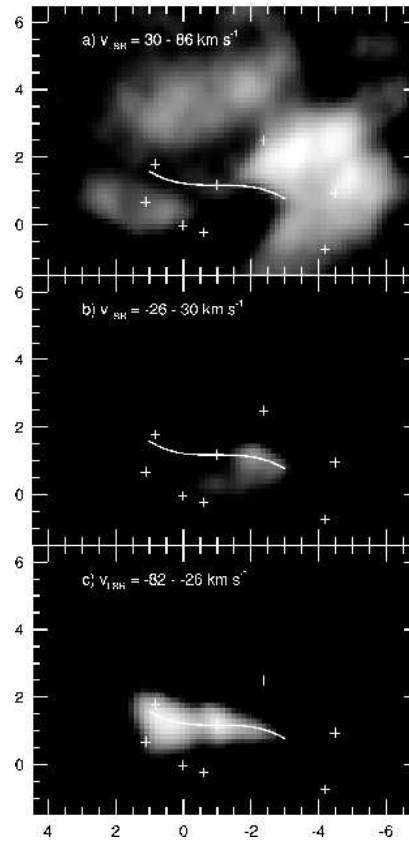


FIG. 4.— Images of [S IV] emission in three velocity intervals. The brightness stretch is linear and the same for all images. Annotations are as in Figure 2. a) Ionized gas near the molecular cloud velocity. We interpret the dark region at bottom center as the region where the cloud surface gas has been disrupted by the jet. b) The ‘bridge’ gas that we interpret as having been accelerated by the jet. c) Blue-shifted emission from the jet which has been ionized by stellar UV radiation. The online movie show the data cube as a sequence of 180 narrow-band images, running from $v_{\text{LSR}} = +85 \text{ km s}^{-1}$ to -82 km s^{-1}